The Iraqi Journal for Mechanical and Material Engineering, Vol.24, No.3, October 2025.

STRUCTURAL BEHAVIOR OF ECO-EFFICIENT GEOPOLYMER CONCRETE BEAM–COLUMN JOINTS UNDER LATERAL MONOTONIC LOADING

Noor Fadhil Jabbar [1] **Ali Mohammed Owaid** [2, *] **Ali Mohammed AL-Araji** [3]
noorfadhil.1989@gmail.com aliowaidali@gmail.com ali_mohammed_ali@atu.edu.iq

[1]Department of Civil Engineering, Faculty Engineering, Razi University, Kermanshah, Iran.
[2]Civil Engineering, Ministry of Electricity, Middle Euphrates Production power, Babylon, Iraq.
[3]Civil Engineering, Department of Civil Techniques, Technical Institute of Babylon, Al-Furat Al-Awsat Technical University, Najaf, Iraq.
[*] Email corresponding author: aliowaidali@gmail.com

ABSTRACT

This study evaluates the seismic performance of exterior beam–column joints (BCJs) made with geopolymer concrete (GPC) as a sustainable alternative to Ordinary Portland Cement (OPC). GPC mixes incorporated Metakaolin (MK) and Ground Granulated Blast Furnace Slag (GGBS) as partial OPC replacements, targeting 30 MPa compressive strength. Three mixes were examined: M1 (control), M2 (60% OPC + 20% GGBS + 20% MK), and M3 (40% OPC + 30% GGBS + 30% MK). Three specimens were tested under monotonic lateral loading to assess cracking, strength, ductility, and energy absorption. Results showed that replacing OPC with GGBS and MK enhanced the seismic performance of BCJs. The control specimen (M1) exhibited brittle shear failure with wide cracks, limited energy dissipation (1461 kN-mm), and moderate ductility (μ = 4.71). In contrast, M2 demonstrated narrower cracks, improved stiffness, higher energy dissipation (1737 kN-mm), and the highest ductility (μ = 5.08), making it the most balanced mix. M3 showed the maximum load capacity (63.2 kN) and highest energy absorption (1851 kN-mm), but with reduced ductility (μ = 4.20), reflecting the brittleness of higher-strength mixes. The enhancements were ascribed to the generation of extra gel phases (C-(A)-S-H and N-A-S-H), which improved the microstructure, bond strength enhancement between the ground structure and the mortar, and stress transfer. Load-displacement curves exhibited a consistent elastic phase followed by progressive ductile failure for the modified mixes. The replacement of 20% of the OPC (M2), overall, showed the best combination of strength and ductility and was the most promising for seismic application. These findings highlight GPC as a high-performance, eco-efficient material that enhances the resilience of BCJs in earthquake-resistant structures while reducing OPC consumption and supporting sustainability.

Received: September 10, 2025.
Accepted: October 07, 2025.

Keywords: Exterior beam column joints, monotonic load, Geopolymer concrete (GPC), Ground Granulated Blast Furnace Slag (GGBS), Metakaolin (MK).

NOMENCLATURE

MK	Metakaolin
GGBS	Ground Granulated Blast Furnace Slag
GPC	Geopolymer concrete
OPC	Ordinary Portland Cement
P_p	Peak monotonic load (kN)
P_f	First crack load (kN)
δ_f	Displacement at first crack load (mm)
δ_p	Displacement at peak monotonic load (mm)
E_{diss}	The energy dissipation capacity (kN-mm)
K	The stiffness (kN/mm)
μ	Ductility factor
P_y	Yield load (kN)
P_u	Ultimate load (kN)
δ_u	Effective ultimate displacement (mm)
δ_y	Yielding displacement (mm)
S.P.	Superplasticizer
F.A.	Fine Aggregate
C.A.	Coarse aggregate

INTRODUCTION

The beam-column joint (BCJ) is a crucial component in reinforced concrete structures, serving as the connection point for transferring forces between the column and beam (Pauletta et al., 2021). Beam-column joints are subjected to a combination of axial, lateral, bending, and shear forces that are complicated and lends itself to damage during seismic loading (Su et al., 2024). In the past, before the 1970s, little research was available to explain or guide design of these joints under seismic loading (Kiran & Genesio, 2014). There was a general conception of analyzing the neighboring beam and column elements that comprise the joint for structural behavior since they have a larger cross-section than the joint (Yang et al., 2024).

However, additional research and post-earthquake investigations show that beam-column connections are typically the weak bottom of the structural system. Damage and failure of beam-column connections are among the leading contributors to structural damage during earthquakes (Shen et al., 2024). Most deteriorated concrete residential buildings were made using traditional concrete, primarily composed of ordinary Portland cement (OPC) derived from limestone. The usage of OPC has resulted in increased carbon dioxide emissions along with depletion of natural materials (Jalal et al., 2025; Sbahieh et al., 2025). This scenario highlights the importance of considering sustainable and eco-friendly alternatives for upgrading or fixing buildings that have suffered earthquake damage, even more so when taking stock of so many older buildings that were built prior to the introduction of modern seismic codes or without earthquake resistant design (Kim et al., 2022; Passoni et al., 2024). However, Geopolymer concrete (GPC) offers a feasible solution. The alkali activation of aluminosilicate minerals such as fly ash and slag produce GPC, which is a sustainable alternative to Portland cement (OPC) (Mostofizadeh & Tee, 2024). GPC is a novel sustainable alternative to Portland cement concrete, made using industrial waste (Chowdhury et al., 2021). GPC effectively reduces carbon dioxide emissions by up to 80 % and is more durable, which makes it a viable option for the built environment (Akbarnezhad et al., 2015; Kumar & Kumar, 2025). GPC has compressive strengths of greater than 80 MPa for structural applications, good acid and sulfate resistance in aggressive environments; it also has superior thermal stability where it retains over 90 % of its compressive strength up to 800 °C (Khasawneh, 2025). GPC has low shrinkage and creep, enhancing durability (Vijai et al., 2010). GPC benefits from rapid development of compressive strength because of improved microstructure during curing (Kishore, 2023).

Geopolymer materials are considered greener than traditional cement. The term 'geopolymer' was coined in 1979 by French researcher Joseph Davidovits, referring to a class of three-dimensional aluminate-silicate compounds derived from materials such as clay, red mud, and fly ash. These materials are created by reacting materials that are rich in alumina-silicate with alkaline liquids, which produces a bond (binder) that has strength, durability, and fire resistance. Geopolymer concrete (GPC) is a type of concrete developed from binder materials (Kalombe et al., 2020). GPC is produced through the reaction of alkaline liquids with silica and alumina-rich minerals, such as fly ash (FA) and ground granulated blast furnace slag (GGBS). This reaction that yields the bonding agent is achieved with the formation of an amorphous polymeric silicate framework made of silica-oxygen-aluminium bonds that are similar in structure to zeolites (Parashar et al., 2022).

According to recent research, geopolymer concrete possesses superior durability and mechanical characteristics when compared to conventional portland cement concrete. It was specifically determined through testing that GPC beams enable significantly greater load-carrying capacity due to improved resistance to bending and torsional forces (Chowdhury et al., 2021). The testing utilized a particular blend of FA geopolymer concrete that incorporated 30% GGBS and established that the microstructure density and mechanical characteristics were improved. Overall, the most favorable results were associated with a mixture containing 30% FA, 30% GGBS, and prepared with 8 M sodium hydroxide solution for the best mechanical characteristics (Sangi et al., 2023).

GPC has many benefits, such as early-age strength, faster setting time, lower density, reduced drying shrinkage, and better early-age static compressive strength. Research into using FA and GGBS with NaOH activation shows that setting time decreased while compressive strength increased (Baqer & Mohammed, 2025). Changing from NaOH concentration of 8 M to 12 M produced notable results, showing 44.3 Mpa compressive strength after 28 days (Ghafoor et al., 2025). A 50% FA and 35% GGB mixture was shown to have the best result, with a quicker setting time and improved strength (Elyamany et al., 2018). FA-GGBS geopolymers also exhibited higher stability against expansion and shrinkage. Therefore, the increase in the material overall durability is another benefit (Samantasinghar & Singh, 2019).

Latest evidence has also shown that GPC beam column joint performs better, according to the seismic response evaluated, than welded reinforced concrete beam column joints (Maniarasan et al., 2023). GPC joints had a better energy dissipation and load capacity. Some studies using a GPC beam column joint reported a strength increase of 32% (Choudhury & Laskar, 2021). However, it is worth noting that GPC cannot alleviate failure in joints located on structures, because failures are attributed to the external forces applied resulting in unexplained premature deterioration. The risk exists that joints could fail under forces above capacity. As a result, there is an increased interest in rehabilitating beam-column joints with advanced innovative materials (Choudhury & Laskar, 2023).

While many studies have investigated the mechanical properties of geopolymer concrete, limited information is available on the behavior of beam-column joints (BCJ) made from geopolymer concrete containing ground granulated blast furnace slag (GGBS) and Metakaolin (MK) under monotonic static loading, especially when it comes to assessing compressive strength and structural performance. To fill the gap in knowledge, a program of experimentation was conducted to assess the mechanical properties and behaviors of geopolymer concrete and evaluate the impacts of relative percentages of FA and GGBS from 20% to 30% as partial substitutes for cement. To further understand the structural behavior of the specimens and development of joint resistance and to interpret the failure mechanisms under lateral actions, the performance of beam-column joints cast with these mixtures was also tested under monotonic lateral loads.

EXPERIMENTAL PROGRAM

Details of the beam-column joint specimens' design, dimensions, and reinforcing

In the experimental program three beam-column joint specimens were fabricated and tested that represent typical exterior beam-column joints that are typically found in multi-story reinforced concrete buildings. The dimensions of the specimens were based on the testing facilities available at the College of Engineering, University of Karbala. The geometrical data displayed in Fig. 1 was used to cast the reinforced concrete joints.

The beams were 200 x 200 mm cross-sectional and 650 mm long, while the columns were 1000 mm high and 250 x 200 mm cross-sectional. The main steel reinforcement for the beams and columns was 12 mm in diameter, while the transversal reinforcement was 6 mm in diameter and 50 mm C/C. The reinforcing features in every sample adhered to ACI 352R and 318 (Farmington Hills, MI, 2019; John F. Bonacci, 2002). Fig. 2 displays the schematic diagrams of each of the samples as well as their dimensions and supporting data. Reinforcement steel bars with widths of 6 and 12 mm were evaluated in a University of Karbala laboratory. The physical characteristics of the reinforcement steel bars are displayed in Table 1 in compliance with ASTM A615 (ASTM A615/AM615-15, 2015).

Fig. 1. Beam-column joints samples.

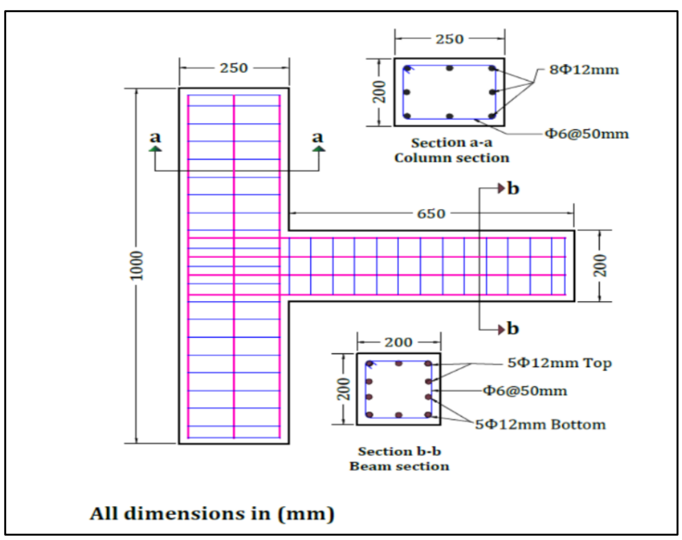

Fig. 2. Schematic illustration of the specimen’s concrete dimensions and reinforcing bar arrangement.

Table 1. Physical properties of steel bars.

Diameter of bars (mm)	Cross sectional area, (mm^2)	Yield strength (MPa)	Tensile strength (MPa)	Maximum tensile strain (%)	Elastic modulus (GPa)
6	28.26	320	475	8	200
12	113.04	415	595	9	210

Binder

Using a Brucker S8 Tiger X-ray fluorescence (XRF) device, the chemical composition of the materials used in this study was examined. Table 2 shows that GGBS is primarily composed of CaO, SiO_2, MgO, and Al_2O_3, whereas MK is primarily composed of SiO_2 and Al_2O_3, and OPC is primarily composed of CaO and SiO_2. As shown in Figure 3, the GGBS's X-ray diffraction (XRD) results showed a broad peak that denoted an amorphous phase that included the phases of quartz (SiO_2) and calcite ($CaCO_3$) within the angular range of (15 to 35) ° 2θ.

A similar analysis of MK's XRD spectrum revealed that its main crystalline phases are quartz (SiO_2) and mullite ($3Al_2O_3 \cdot 2SiO_2$), with trace amounts of hematite (Fe_2O_3), anatase (TiO_2), and the compound tricalcium silicate (C_3S), also shown in Fig. 3.

The metakaolin sample has a high aluminosilicate concentration, as evidenced by the about 97.81% total content of hematite Fe_2O_3, SiO_2, and Al_2O_3. For aluminosilicate materials to be deemed appropriate for the creation of geopolymer gels, they must make up at least 70% of the overall composition, as per ASTM C618-17 (ASTM 618/C618-17, 2017). It is established that metakaolin is a suitable precursor for the synthesis of geopolymers since it surpasses this criterion.

Table 2. Properties and Chemical compositions of MK, GGBS and OPC.

Compound	MK (wt%)	GGBS (wt%)	OPC (wt%)
SiO_2	50.36	35.99	21.49
Al_2O_3	44.52	9.75	4.08
Fe_2O_3	1.25	0.72	3.25
CaO	0.73	38.88	63.71
MgO	0.89	7.36	2.05
SO_3	0.08	1.98	1.96
Na_2O	0.06	0.42	0.65
K_2O	-	0.07	1.05
R_2O^*	-	0.19	1.34

TiO_2	0.55	-	-
L.O.I.	1.4	2.9	0.39
Specific surface area (m^2/kg)	20,450	415	320
Density (g/cm^3)	2.45	2.65	3.12

* $R_2O = Na_2O + 0.658K_2O$

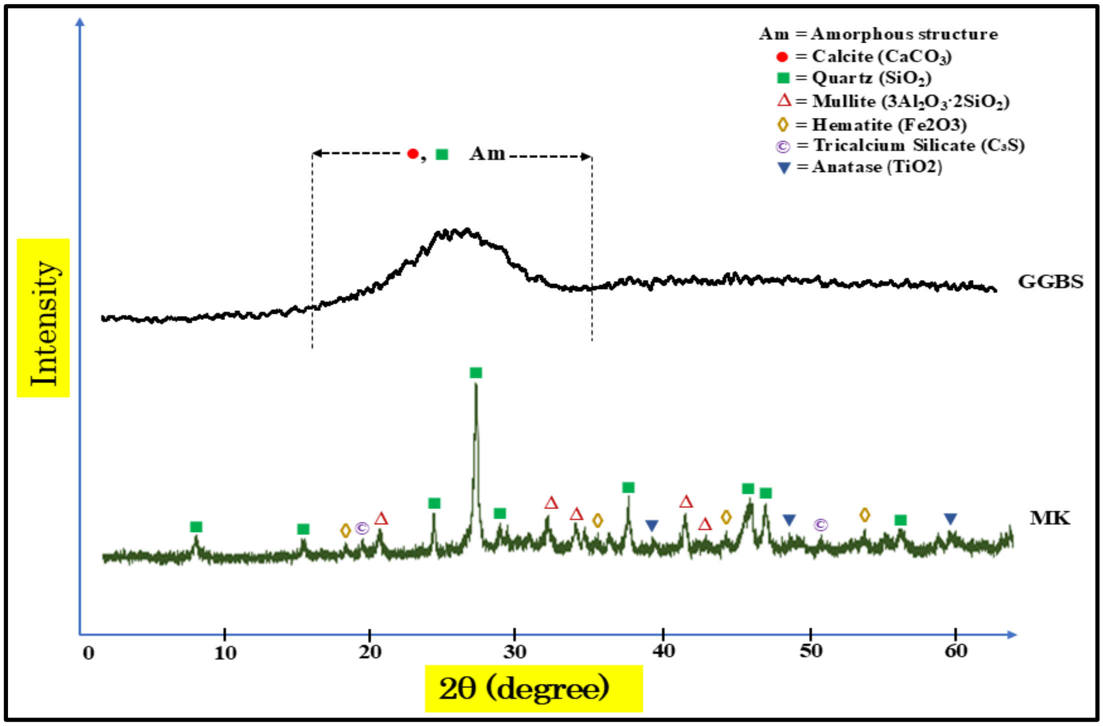

Fig. 3. XRD patterns of GGBS and MK in this study.

Aggregates

The fine aggregate employed in this research was obtained from Karbala, Iraq. The fine aggregate had a maximum nominal particle size of 4.75 mm and unit weight equal to 1625 kg/m3, whereas the fine aggregate showed specific gravity equal to 2.65, fineness modulus equal to 2.75, and total water absorption equal to 2.35%. Meanwhile, the coarse aggregate underwent crushing and was also imported from Baghdad, Iraq, with a unit weight of 1520 kg/m3 and a maximum nominal particle size of 9.5 mm. The coarse aggregate had a fineness modulus of 6.10, specific gravity of 2.55, and water absorption equal to 1.79%.

To check quality, gradation testing is done based on ASTM C33 (ASTM C33/C33M-16, 2016). This determines which the specific distribution of the particles necessary to provide the required concrete properties. The aggregate gradations of the ag-" fine and coarse" are displayed in Fig. 4.

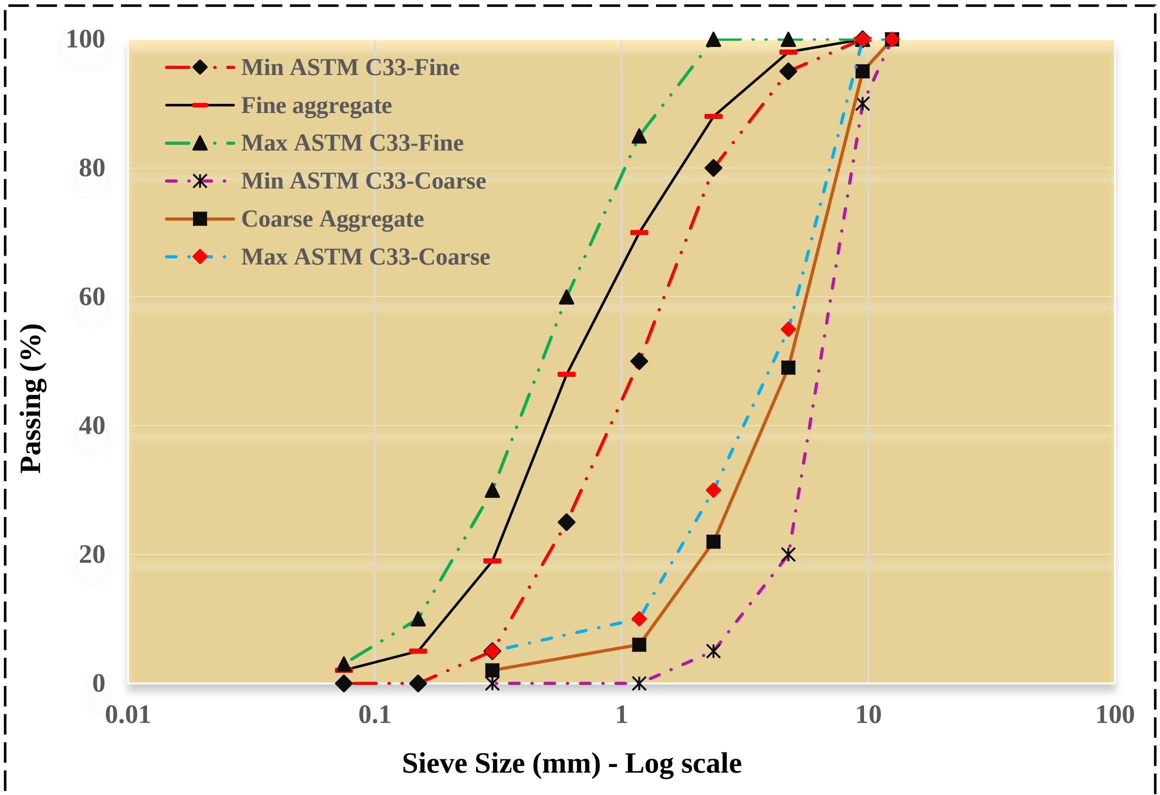

Fig. 4. Gradation curves for Fine and Coarse Aggregates.

Materials

Solutions of NaOH and Na2SiO3 were employed in this investigation as alkaline activators at a mass ratio of 1:2.5. Based on published research (Ryu et al., 2013; Sumajouw et al., 2007) showing how well it improves the performance of geopolymer concrete, this ratio was chosen. In order to create a solution with a concentration of 10 M, 98% pure NaOH pellets were first dissolved in distilled water. The NaOH solution was then mixed with a Na_2SiO_3 solution, which had 42% solids and 58% liquid. The alkali-activated solution (AAS) that is produced is essential for the synthesis of geopolymers and for giving concrete its mechanical qualities. Aluminum and silicon dissolve when combined with geopolymer precursors to generate oligomeric aluminosilicates, which subsequently polymerize into a three-dimensional network structure that solidifies over time.

The generated binder gel controls the concrete's strength properties and holds the granules together. To increase the alkaline activator solution's reactivity, the alkaline activators were made in the proper ratios 24 hours prior to casting. Heat was released as the polymerization process began when the NaOH solution and the Na_2SiO_3 solution were combined. To guarantee reaction stability and efficient mixing, the mixture was thus allowed to cool for an hour before being added to the dry mix.

In accordance with ASTM C494-05 (ASTM C494/C494-05, 2005), to improve workability without the use of water, a superplasticizer admixture called Master Glenium-54 was added at a rate of 1.2% by binder weight.

Conditions for sample preparation and curing

The geopolymer concrete was made in the lab under standard room conditions using a method similar to that previously described (Baskara Sundararaj et al., 2022). To make a uniform blend, the dry materials (OPC, MK, and GGBS) were combined with fine and coarse aggregates in a dry environment for three minutes using a mechanical mixer. The water mixture for OPC mixing or the alkaline activation solution for GPC mixtures and superplasticizer were then added to improve workability. The ultimate consistency was then achieved after five minutes of mix.

After mixing, three layers of the newly mixed concrete were poured into the molds, compressed to liberate trapped air using a vibration table, and then put through fresh state tests, as shown in Fig. 5. They removed the molds after a day, wrapped the specimens in plastic, and let them cure at room temperature (23 ± 2 °C) until the dry state examination.

Fig. 5. Stages of material mixing, slump testing, and casting specimens in the laboratory.

Mix Details

The aim of the study was to construct geopolymer concrete mixes with a compressive strength grade of GP30 by substituting ground granulated blast furnace slag (GGBS) and metakaolin (MK) for some of the cement. The investigation included two mixes, where the replacement ratios of MK and GGBS relative to the total mass of cement were (20 and 30)

%. The mixes were labeled based on the OPC ratio as the first number, the GGBS content as the second number, and the MK replacement ratio as the third number. The details of the geopolymer concrete mixes for this study are presented in Table 3.

Table 3. Mix Proportions of GPC blends.

Mix No.	**Mix Notation**	**W/C or L/B**	**Quantities of ingredients (kg/m^3)**							
			OPC	**GGBS**	**MK**	**NaOH**	**Na_2SiO_3**	**F.A.**	**C.A.**	**S.P. (1.2% weight of binder or cement)**
M1	OPC-Control	0.52	360	0	0	0	0	635	1105	4.32
M2	OPC60G20MK20	0.52	216	72	72	55.70	139.25	650	1105	4.32
M3	OPC40G30MK30	0.52	144	108	108	55.70	139.25	650	1105	4.32

The loading boundary conditions

In a moment frame structure, when lateral loads are applied, the mid-span moments of the members are practically nonexistent. Thus, if outside connections were considered a moment frame structure, the confinement requirements would be similar to those in Fig. 6. Whereas a hinge supports the bottom of the column, a roller supports the bottom of the beam. In compliance with the ACI T1.1 (Norman L. Scott NMH, Michael E. Kreger, 2001) and previous studies (Alhaddad et al., 2012; Azimi et al., 2014; Melo et al., 2021, 2022; Wang et al., 2022), a well-established standard quasi-static cycle pattern and modeling setup were employed for the tests. Figure 6 shows a schematic diagram for laboratory testing of the specimen that specifies the boundary requirements for this research.

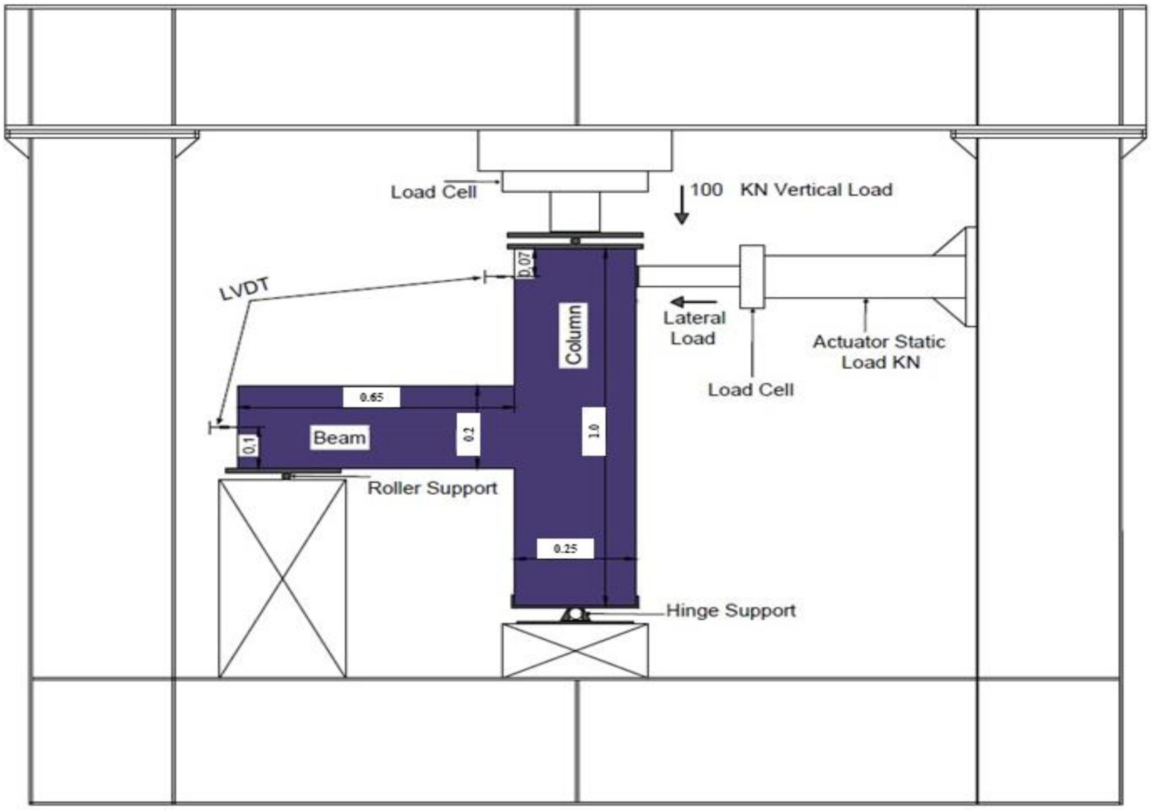

Fig. 6. Schematic diagrams Experimental setup showing the prototype structure and applied loading protocol.

Instrumentation and test protocol

The cyclic load has been the subject of much prior investigation. However, a new experiment was carried out to investigate how concrete structures under monotonic stress circumstances were affected by seismic design improvement techniques. Even though cyclic loading is more common during earthquakes, the University of Kerbala's testing lab could only withstand monotonic static stress. To apply a constant axial force of 0.08*Ac*fc` = 100 kN, a fixed load cell attached to a hydraulic jack is used. A single-direction lateral monotonic load is applied by a load cell positioned on a horizontal jack at the top of the column, 70 mm from the column face. There is no change in the load until complete failure. There were two places where the specimen was fastened to the universal load frame. One characteristic is a hinged support at the base of the column, which is accomplished by skillfully setting a base that is immobile on top of the device's structure and welding smooth strengthened steel. The column compresses and the specimen stays stationary when the upper portion of the column sample is subjected to axial load. In order to maintain the model stable during inspection, the second point uses a steel structure with a roller support 70 mm from the beam face to support the specimen from the beam side .

The LVDT, which monitors displacement changes, was only installed 70 mm from the column face, close to the lateral monotonic load. The specimen's preparation and analysis in the lab are shown in Figure 7. Axial monotonic loads were applied initially once the model was secured, and then subsequently. The displacement of the models at failure was then measured. Each specimen's load-displacement curve was plotted.

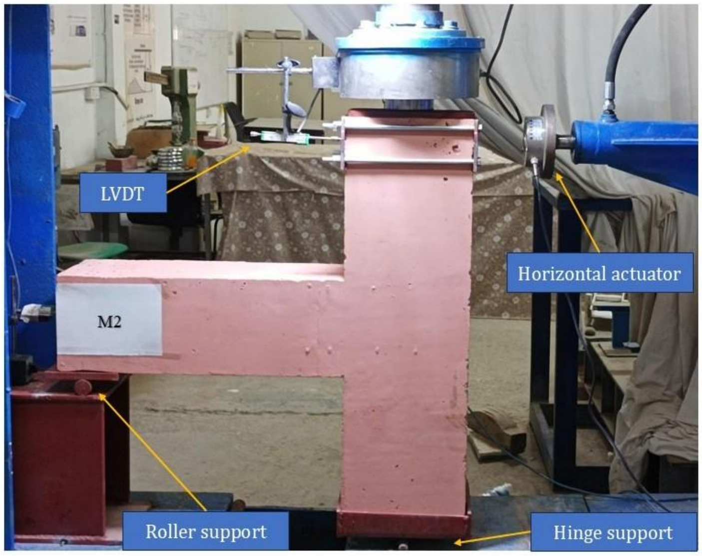

Fig. 7. An image of the laboratory's test setup and specimen

RESULTS AND DISCUSSIONS

Peak Monotonic Load and crack pattern

Table 4 shows the first crack load, displacement in the first crack loads, peak monotonic loads, and displacement at the peak monotonic loads for specimens of beam-column joints subjected to monotonic lateral loading. According to the test results, the control mixture (M1) cracked at a displacement of 2.2 mm and an initial load of 18 kN, peaking at 54.2 kN and 35.6 mm. On the other hand, mix (M2), which was composed of 60% Portland cement, 20% slag, and 20% metakaolin, showed a significant improvement: higher initial stiffness and a higher capacity to withstand loads before cracking were indicated by the first cracking load increasing to 24 kN with a displacement of 2.7 mm and the peak load reaching 57.3 kN with a displacement of 39.6 mm.

Mix (M3), consisting of 40% cement, 30% slag, and 30% metakaolin, demonstrated the best performance. The first cracking load rose to 27 kN with a displacement of 3.1 mm, and the peak load reached 63.2 kN at a displacement of 40.1 mm, reflecting a higher resistance to cracking and an increased ability to sustain ultimate loads, along with greater energy absorption up to the peak. Overall, the addition of slag and metakaolin improved the concrete’s cracking resistance and energy absorption capacity, with mix (M3) showing the most superior performance, while mix (M2) provided a significant enhancement in initial crack resistance and stiffness.

Table 4. loads at peak and first crack of the specimens

Mix No.	Mix Notation	P_f (kN)	δ_f (mm)	P_P (kN)	δ_p (mm)
M1	OPC-Control	18	2.2	54.2	36.6
M2	OPC60G20MK20	24	2.7	57.3	38.1
M3	OPC40G30MK30	27	3.1	63.2	40.1

The failure results in Fig. 8, indicated that the control specimen M1 (conventional concrete) experienced brittle failure characterized by wide and early shear cracks concentrated in the joint region, reflecting weak bonding in the interfacial transition zone and limited capacity to resist crack propagation. In contrast, specimen M2 with partial replacement by MK and GGBS exhibited an improved failure mode, where the cracks appeared narrower and developed more gradually, indicating higher resistance to crack initiation and better ductility. Specimen M3 with higher replacement levels demonstrated the most favorable behavior, with finer, more numerous, and uniformly distributed cracks across the joint region, reflecting a ductile and progressive failure mode with greater energy absorption capacity. These observations are consistent with previous studies (Naik et al., 2015; Nath & Sarker, 2014; Shakir & Dawood, 2024; Velastegui et al., 2024), which reported that incorporating MK with GGBS enhances the microstructure, reduces porosity, and leads to the formation of additional gel phases (C-A-S-H and N-A-S-H). Such improvements strengthen interfacial bonding, delay brittle failure, and enhance the shear and flexural performance of concrete.

Fig. 8. Experimental specimens' crack patterns.

Load-Displacement Curves

The load–displacement curves of beam–column joints made of geopolymer concrete (GPC) demonstrated clear superiority over conventional cement concrete, particularly in crack

resistance and flexibility under high loads, as shown in Fig. 9. During the initial loading stages, specimens showed stable linear elastic responses, which was attributed to the densely compacted, low-porosity microstructure of the geopolymer matrix. With the increase of load, cracks were more and more discrete, slow but uniform, energy absorption was high and failure was retarded. The pozzolanic reaction between metakaolin and slag contributed also in enhancing the performance by generating more gel products (C-A-S-H and N-A-S-H) which can fill voids and improve the interfacial bond between matrix and reinforcement and thus stress could distributed incrementally until stress reached its maximum level. The reinforcement yielded and the displacement increased until rupture; however, failure was gradual and ductile, not abrupt and brittle. These results are consistent with the world literature (Deb et al., 2014; Imtiaz et al., 2020; Haiyan Zhang et al., 2021), which is an indication that geopolymer concrete behaves ductile and also improves the lateral load resistivity considering the denser microstructure and highly efficient gel products.
As the concrete takes on the applied load and reaches its ultimate bending capacity at (a), the beam–column joint reacts by opening tension cracks. The joint is stabilized by the resistance of the rebar to tensile forces in the segment (a) – (b). The capacity of the joint to carry load is becoming close to the upper limit at (b). Beyond (b) the reinforcement starts to yield with a rapid increase in bending until (c), where the joint finally fails.

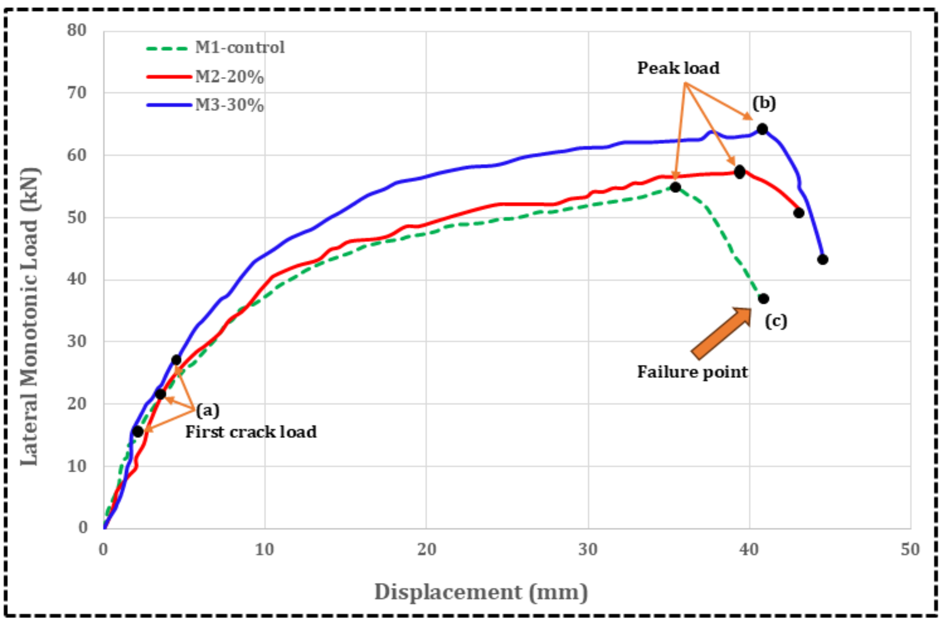

Fig. 9. Load-displacement curves for experimental specimen

Energy Dissipation and Stiffness

The seismic performance of beam–column joints is strongly governed by their ability to dissipate energy and to retain stiffness during lateral loading. Energy dissipation (E_{diss}) represents the cumulative capacity of the joint to absorb and release inelastic deformation energy, which is a fundamental measure of ductility and earthquake resistance. In practice, Ediss is quantified as the total enclosed area beneath the experimental load–displacement curve, starting from the onset of inelastic behavior until structural collapse. This parameter is mathematically expressed as the integral of force with respect to displacement, and its numerical evaluation is commonly achieved through the trapezoidal approximation method, as widely reported in seismic performance studies (Hakuto et al., 2000; Park, 1989).

The energy dissipation capacity (E_{diss}) is quantified as the area under the force–displacement curve. This value can be determined numerically by applying the trapezoidal integration method, as expressed in Eq. 1.

$$E_{diss} = \int_0^{\delta max} P(\delta).d\delta \approx \sum_0^{\delta_{i+1} = \delta max} \left((\frac{P_{i+1} + P_i}{2}) \text{ x } (\delta_{i+1} - \delta_i) \right) \quad (1)$$

Where Pi and δi represent the applied force and measured lateral displacement, respectively, at each displacement level, i.

Equally important is the stiffness index (K), which provides insight into the structural rigidity and the ability of the joint to control lateral deformation. Defined as the ratio between the peak load and the corresponding peak displacement (Sakthimurugan & Baskar, 2021; Ugale & Khante, 2020), stiffness serves as a direct indicator of the joint’s stability under cyclic or monotonic loading. Higher stiffness values correlate with improved resistance against lateral drift, thereby reducing potential seismic vulnerability (X. Zhang & Li, 2021). The K value is determined using Eq. 2.

$$K = \frac{Pp}{\delta p} \quad (2)$$

The table results indicate that the specimens containing slag and metakaolin (M2 and M3) clearly outperformed the control specimen (M1) in terms of peak load, deformability, and energy dissipation. The maximum load increased from 54.2 kN in the control specimen to 57.3 kN and 63.2 kN at 20% and 30% replacement ratios, respectively. This improvement is attributed to the formation of additional hydration products, such as C-(A)-S-H and N-A-S-H, resulting from the reaction between slag and metakaolin with the alkaline activator solution, which enhances microstructural bonding and increases strength (Li et al., 2023; Mostofizadeh & Tee, 2024).

The displacement at peak load also gradually increased (from 36.6 mm to 40.1 mm), indicating improved ductility. This is due to the semi-glassy nature of slag, which facilitates better stress transfer within the concrete matrix (Mao et al., 2023). Regarding energy dissipation, it increased by approximately 27% compared to the control mix, demonstrating the enhanced ability of these mixes to absorb and dissipate energy under lateral loads—a critical factor for improving the seismic performance of joints (Saranya et al., 2021). The initial stiffness showed a slight increase from 1.48 to 1.57 kN/mm, attributed to the higher micro-density resulting from the good packing of geopolymeric products. However, the increase was relatively limited due to the simultaneous rise in deformability, which reduces the overall slope of the load–displacement curve. Therefore, it can be concluded that partially replacing ordinary Portland cement with slag and metakaolin improves the mechanical and dynamic properties of concrete joints, making them more efficient in resisting seismic loads.

Table 5. Experimental Results of cumulative energy dissipation and stiffness for specimens

Mix No.	**Mix Notation**	**P_p (kN)**	**δ_p (mm)**	**E_{diss} (kN-mm)**	**K (kN/mm)**
M1	OPC-Control	54.2	36.6	1461	1.48
M2	OPC60G20MK20	57.3	38.1	1737	1.50
M3	OPC40G30MK30	63.2	40.1	1851	1.57

Displacement Ductility

Ductility is commonly quantified through numerical indices such as the ductility factor or ductility ratio, which reflect a structure's ability to undergo plastic deformation before failure (Sakthimurugan & Baskar, 2021). Two main forms of ductility factor are recognized: curvature ductility and displacement ductility. In this work, the displacement ductility factor was adopted since both reinforcing steel and concrete exhibit nonlinear behavior, resulting in multiple yielding points and load steps (da Silva et al., 2023).

The determination of the yielding point follows a bilinear approximation of the load–displacement response, as illustrated in Fig. 10 (Deng et al., 2022; Owaid et al., 2026). The yield displacement is defined at either the material failure or when the load capacity is reduced to 85% of the maximum load, according to well-known procedures (Park, 1989; Vamvatsikos & Aschheim, 2016). The displacement ductility factor μ is computed as the ratio of the effective ultimate displacement to the yield displacement which can be written as follows Eq. 3. This quantity is a straightforward, informative measure of the ability of a structural system to sustain large deformations with sufficient strength, which is of paramount importance in seismic design and evaluation.

$$\mu = \frac{\delta_u}{\delta_y} \qquad (3)$$

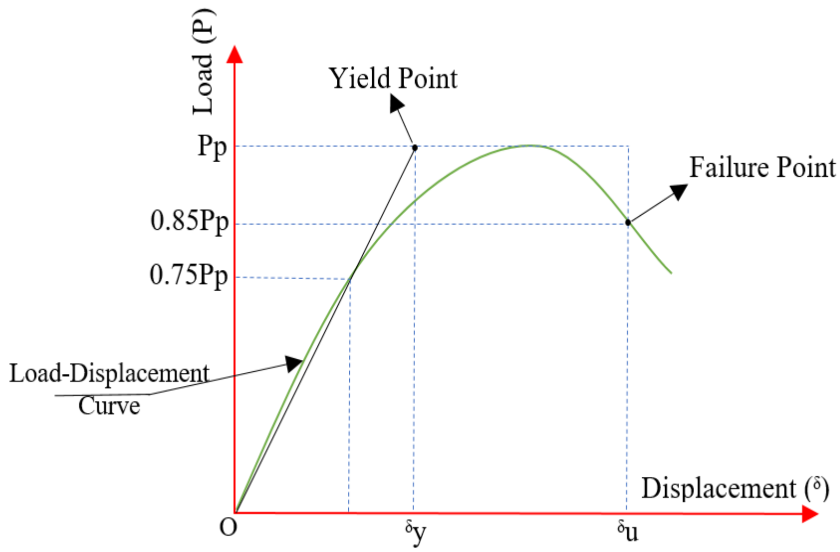

Fig. 10. Load-displacement curves points description (Deng et al., 2022; Owaid et al., 2026).

Table 6. Results of ductility factor for specimens.

Mix No.	Mix Notation	P_p (kN)	P_y (kN)	δ_y (mm)	P_u (kN)	δ_u (mm)	μ
M1	OPC-Control	54.2	34.02	8.1	46.07	38.2	4.71
M2	OPC60G20MK20	57.3	38.70	8.8	48.70	44.7	5.08
M3	OPC40G30MK30	63.2	43.90	10.6	53.72	44.6	4.20

Where: P_u = 85% * P_p

The analysis of ductility factors in Table 6 shows that the control mix (M1) exhibited a ductility factor of 4.71, whereas the mix with 20% replacement of slag and metakaolin (M2) achieved the highest ductility factor of 5. This indicates its superior ability to accommodate deformations and gradually dissipate energy prior to failure. This improvement may be because of the creation of more hydration products (C-(A)-S-H and N-A-S-H), which improved microstructural bonding and distribution of internal stresses in the concrete matrix (Hosen et al., 2022). As noted earlier, however, while M3 produced the highest peak load (63.2 kN), it had a lower ductility factor (4.20) and this supports the well-known observation that high-strength concrete is more brittle and has less capability to plastic deformation than its lower strength counterpart (Kwan & Ho, 2010).

Several previous studies also highlight that ductility is improved when balance between strength and deformability is used, thereby moderate replacement ratios and lateral confinement are balancin means of improving seismic performance (Taheri et al., 2017).
Therefore, it can be concluded that a 20% replacement ratio provides the optimal balance between mechanical strength and ductility, making it the most efficient mix for enhancing the seismic resilience of concrete joints.

CONCLUSIONS

The behavior of reinforced external beam–column joint specimens under monotonic lateral loading was experimentally investigated by preparing three test samples (M1, M2, and M3). The main findings and observations from the study can be summarized as follows:

- Partial replacement of Ordinary Portland Cement (OPC) with Ground Granulated Blast Furnace Slag (GGBS) and Metakaolin (MK) enhanced crack resistance and increased the peak load compared to the control mix (M1).
- Mix M2 (20% replacement) achieved the best balance between strength and ductility, recording the highest ductility factor ($\mu = 5.08$).
- Mix M3 (30% replacement) exhibited the highest peak load (63.2 kN) and the greatest energy dissipation capacity (1851 kN-mm), but recorded lower ductility ($\mu = 4.20$), indicating a more brittle behavior.
- The inclusion of pozzolanic materials promoted the formation of additional gel products (C-(A)-S-H and N-A-S-H), which improved the microstructural bonding and increased energy dissipation by approximately 27%.
- A replacement rate of 20% can be considered the most efficient for enhancing the seismic performance of beam–column joints.

PRACTICAL RECOMMENDATIONS

Based on the experimental results and analysis:

- The optimal partial replacement ratio of Ordinary Portland Cement is 20% GGBS + 20% MK, as it provides the best balance between strength and ductility—two critical factors in enhancing the seismic resistance of structural systems.
- The 30% substitution mixture (M3) is appropriate for applications with higher peak loads and more energy absorption, but the decrease in ductility that comes with it should be taken into account when designing structures.
- The geopolymer mixture (M2) is proposed for application in areas of high seismicity, as it showed the best balanced performance against cracking and abrupt failure.
- The results of this investigation may be exploited in the design of exterior beam–column joints in earthquakeresistant buildings leading to enhanced structural safety

and less dependency on conventional Portland cement— and thus promoting environmental sustainability as well.

STUDY LIMITATIONS

An important limitation is the entire test program is based on monotonic lateral loading rather than cyclic loading. This limitation was due to the lack of specialized equipment for conducting cyclic loading tests in the laboratory. Although monotonic loading has its advantages in initial stiffness, maximum load-bearing capacity, cracking pattern, cracking propagation and so on, it cannot reflect hysteretic behavior, energy dissipation capability and degradation traits under cyclic loading as in seismic event. Interpretation of the results with respect to this limitation is recommended and future work including cyclic testing would better quantify the seismic performance of the proposed beam–column joint arrangements.

REFERENCES

Akbarnezhad, A., Huan, M., Mesgari, S., & Castel, A. (2015). Recycling of geopolymer concrete. Construction and Building Materials, 101, 152–158. https://doi.org/10.1016/j.conbuildmat.2015.10.037.

Alhaddad, M. S., Siddiqui, N. A., Abadel, A. A., Alsayed, S. H., & Al-Salloum, Y. A. (2012). Numerical investigations on the seismic behavior of FRP and TRM upgraded RC exterior beam-column joints. Journal of Composites for Construction, 16(3), 308–321. https://doi.org/10.1061/(ASCE)CC.1943-5614.0000265.

ASTM 618/C618-17. (2017). Standard Specification for Coal Fly Ash and Raw or Calcined Natural Pozzolan for Use in Concrete. American Society for Testing and Materials.

ASTM A615/AM615-15. (2015). Standard Specification for Deformed and Plain Carbon-Steel Bars for Concrete Reinforcement. American Society for Testing and Materials.

ASTM C33/C33M-16. (2016). Standard specification for concrete aggregate. American Society for Testing and Materials.

ASTM C494/C494-05. (2005). Standard specification for chemical admixtures for concrete. American Standard for Testing and Materials; West Conshohocken, Pennsylvania, USA.

Azimi, M., Adnan, A. Bin, Bin Mohd Sam, A. R., Tahir, M. M., Faridmehr, I., & Hodjati, R. (2014). Seismic performance of RC beam- column connections with continuous rectangular spiral transverse reinforcements for low ductility classes. The Scientific World Journal, 2014(1), 802605. https://doi.org/10.1155/2014/802605.

Baqer, B. T., & Mohammed, A. S. (2025). Evaluating the compressive strength of fly ash-slag-based geopolymer concrete: impact of hydraulic, silica, alumina, and lime moduli, and sodium silicate using various predictive models. Innovative Infrastructure Solutions, 10(5), 191. https://doi.org/10.1007/s41062-025-01973-4.

Baskara Sundararaj, J., Kannan Rajkumar, P. R., Sivasakthi, M., & Jegan, M. (2022). Effect of mineral admixtures on mechanical and thermal properties of geopolymer mortar at elevated temperature. Innovative Infrastructure Solutions, 7(6), 354. https://doi.org/10.1007/s41062-022-00947-0.

Choudhury, A. H., & Laskar, A. I. (2021). Rehabilitation of substandard beam-column joint using geopolymer. Engineering Structures, 238, 112241. https://doi.org/10.1016/j.engstruct.2021.112241.

Choudhury, A. H., & Laskar, A. I. (2023). Rehabilitation of Exterior Beam-Column Joint by Geopolymer Mortar under Quasi-Static Loading. ACI Structural Journal, 120(5), 49–62. https://doi.org/10.14359/51738835.

Chowdhury, S., Mohapatra, S., Gaur, A., Dwivedi, G., & Soni, A. (2021). Study of various properties of geopolymer concrete–A review. Materials Today: Proceedings, 46(11), 5687–5695. https://doi.org/10.1016/j.matpr.2020.09.835.

da Silva, A. H. A., Tsiavos, A., & Stojadinović, B. (2023). Ductility-strength and strength-ductility relations for a constant yield displacement seismic design procedure. Bulletin of Earthquake Engineering, 21(9), 4449–4479. https://doi.org/10.1007/s10518-023-01683-1.

Deb, P. S., Nath, P., & Sarker, P. K. (2014). The effects of ground granulated blast-furnace slag blending with fly ash and activator content on the workability and strength properties of geopolymer concrete cured at ambient temperature. Materials & Design (1980-2015), 62, 32–39. https://doi.org/10.1016/j.matdes.2014.05.001.

Deng, B.-Y., Liu, X., Yu, K.-Q., Li, L.-Z., & Chen, Y. (2022). Seismic retrofitting of RC joints using steel cage and haunch with bolted steel plate. Structures, 43, : : 285-298. https://doi.org/10.1016/j.istruc.2022.06.056.

Elyamany, H. E., Abd Elmoaty, M., & Elshaboury, A. M. (2018). Setting time and 7-day strength of geopolymer mortar with various binders. Construction and Building Materials, 187, 974–983. https://doi.org/10.1016/j.conbuildmat.2018.08.025.

Farmington Hills, MI, U. (2019). Building Code Requirements for Structural Concrete and Commentary. American Concrete Institute, ACI 318-19, 628.

Ghafoor, M. T., Ali, S., Imran, M., & Saeed, M. (2025). Impact of sodium hydroxide molarity on mechanical properties of fly ash–slag-based geopolymer concrete. Proceedings of the Institution of Civil Engineers-Structures and Buildings, 178(4), 402–411. https://doi.org/10.1680/jstbu.24.00169.

Hakuto, S., Park, R., & Tanaka, H. (2000). Seismic load tests on interior and exterior beam-column joints with substandard reinforcing details. Structural Journal, 97(1), 11–25. https://doi.org/10.14359/829.

Hosen, M. A., Shammas, M. I., Shill, S. K., Al-Deen, S., Jumaat, M. Z., & Hashim, H. (2022). Ductility enhancement of sustainable fibrous-reinforced high-strength lightweight concrete. Polymers, 14(4), 727. https://doi.org/10.3390/polym14040727.

Imtiaz, L., Rehman, S. K. U., Ali Memon, S., Khizar Khan, M., & Faisal Javed, M. (2020). A Review of Recent Developments and Advances in Eco-Friendly Geopolymer Concrete. Applied Sciences, 10(21). https://doi.org/10.3390/app10217838.

Jalal, P. S., Srivastava, V., & Tiwari, A. K. (2025). Portland Cement at the Crossroads: Environmental Imperatives and Pathways to Sustainable Production. Journal of Mechanical and Civil Engineering, 22(4), 1–10. https://doi.org/10.9790/1684-2204010110.

John F. Bonacci, S. M. A. (2002). Recommendations for Design of Beam-Column Connections in Monolithic Reinforced Concrete Structures. American Concrete Institute, ACI 352R-02, 1–37.

Kalombe, R. M., Ojumu, V. T., Eze, C. P., Nyale, S. M., Kevern, J., & Petrik, L. F. (2020). Fly ash-based geopolymer building materials for green and sustainable development. Materials, 13(24), 5699. https://doi.org/10.3390/ma13245699.

Khasawneh, M. A. (2025). Geopolymer concrete in construction projects: a review. Discover Civil Engineering, 2(1), 1–20. https://doi.org/10.1007/s44290-025-00281-1.

Kim, J.-H., Hessek, C. J., Kim, Y. J., & Park, H.-G. (2022). Seismic analysis, design, and retrofit of built-environments: a procedural review of current practices and case studies. Journal of Infrastructure Preservation and Resilience, 3(1), 11. https://doi.org/10.1186/s43065-022-00056-3.

Kiran, R., & Genesio, G. (2014). A case study on pre 1970s constructed concrete exterior beam-column joints. Case Studies in Structural Engineering, 1, 20–25. https://doi.org/10.1016/j.csse.2014.04.002.

Kishore, K. (2023). Geopolymer concrete and its strength influencing variables. Materials Today: Proceedings, 80, 1434–1441. https://doi.org/10.1016/j.matpr.2023.01.225.

Kumar, T. U., & Kumar, M. V. (2025). Influence of geopolymer aggregate on the durability, mechanical characteristics and chemical properties of concrete. Journal of Building Pathology and Rehabilitation, 10(2), 148. https://doi.org/10.1007/s41024-025-00654-0.

Kwan, A. K. H., & Ho, J. C. M. (2010). Ductility design of high-strength concrete beams and columns. Advances in Structural Engineering, 13(4), 651–664. https://doi.org/10.1260/1369-4332.13.4.651.

Li, J., Dang, X., Zhang, J., Yi, P., & Li, Y. (2023). Mechanical properties of fly ash-slag based geopolymer for repair of road subgrade diseases. Polymers, 15(2), 309. https://doi.org/10.3390/polym15020309.

Maniarasan, S. K., Chandrasekaran, P., Jayaprakash, S., & Ravindran, G. (2023). Influence of slag-based geopolymer concrete on the seismic behavior of exterior beam column joints. Sustainability, 15(3), 2327. https://doi.org/10.3390/su15032327.

Mao, Y., Du, Y., Hwang, H., Su, J., Hu, X., Liu, Y., & Shi, C. (2023). Seismic performance of interior beam- column joints using reinforced slag- based geopolymer concrete. Earthquake Engineering & Structural Dynamics, 52(2), 285–307. https://doi.org/10.1002/eqe.3760.

Melo, J., Pohoryles, D. A., Rossetto, T., & Varum, H. (2021). Full-scale cyclic testing of realistic reinforced-concrete beam-column joints. MethodsX, 8, : : 101409. https://doi.org/10.1016/j.mex.2021.101409.

Melo, J., Varum, H., & Rossetto, T. (2022). Experimental assessment of the monotonic and cyclic behaviour of exterior RC beam-column joints built with plain bars and non-seismically designed. Engineering Structures, 270, 114887. https://doi.org/10.1016/j.engstruct.2022.114887.

Mostofizadeh, S., & Tee, K. F. (2024). Review of next-generation earthquake-resistant geopolymer concrete. Discover Materials, 4(1), 62. https://doi.org/10.1007/s43939-024-00132-3

Naik, M. L. R., B, P. M. N., & .K, D. A. (2015). Study on Flexural Behavior of Fly Ash based Reinforced Rectangular Geopolymer Concrete Slabs. International Journal of Engineering Research & Technology (IJERT), 4(9), 523–528.

Nath, P., & Sarker, P. K. (2014). Effect of GGBFS on setting, workability and early strength properties of fly ash geopolymer concrete cured in ambient condition. Construction and Building Materials, 66, 163–171. https://doi.org/10.1016/j.conbuildmat.2014.05.080.

Norman L. Scott NMH, Michael E. Kreger, L. D. M. (2001). Commentary on Acceptance Criteria for Moment Frames Based on Structural Testing. American Concrete Institute, ACI T1.1-01.

Owaid, A. M., Akhaveissy, A. H., & Al-Abbas, B. H. (2026). Retrofitting Seismically Designed Exterior Beam-Column Joints under Lateral Monotonic Loading: A Numerical Analysis Based on Experimental Testing. Journal of Rehabilitation in Civil Engineering, 14(1). https://doi.org/10.22075/jrce.2024.33704.2043.

Parashar, A. K., Sharma, P., & Sharma, N. (2022). Effect on the strength of GGBS and fly ash based geopolymer concrete. Materials Today: Proceedings, 62, 4130–4133. https://doi.org/10.1016/j.matpr.2022.04.662.

Park, R. (1989). Evaluation of ductility of structures and structural assemblages from laboratory testing. Bulletin of the New Zealand Society for Earthquake Engineering, 22(3), 155–166. https://doi.org/10.5459/bnzsee.22.3.155-166.

Passoni, C., Caruso, M., Felicioni, L., & Negro, P. (2024). The evolution of sustainable renovation of existing buildings: from integrated seismic and environmental retrofitting strategies to a life cycle thinking approach. Bulletin of Earthquake Engineering, 22(13), 6327–6357. https://doi.org/10.1007/s10518-024-01991-0.

Pauletta, M., Di Marco, C., Frappa, G., Miani, M., Campione, G., & Russo, G. (2021). Seismic behavior of exterior RC beam-column joints without code-specified ties in the joint core. Engineering Structures, 228, 111542. https://doi.org/10.1016/j.engstruct.2020.111542.

Ryu, G. S., Lee, Y. B., Koh, K. T., & Chung, Y. S. (2013). The mechanical properties of fly ash-based geopolymer concrete with alkaline activators. Construction and Building Materials, 47, 409–418. https://doi.org/10.1016/j.conbuildmat.2013.05.069.

Sakthimurugan, K., & Baskar, K. (2021). Experimental investigation on rcc external beam-column joints retrofitted with basalt textile fabric under static loading. Composite Structures, 268, : : 114001. https://doi.org/10.1016/j.compstruct.2021.114001.

Samantasinghar, S., & Singh, S. P. (2019). Fresh and hardened properties of fly ash–slag blended geopolymer paste and mortar. International Journal of Concrete Structures and Materials, 13(1), 47. https://doi.org/10.1186/s40069-019-0360-1.

Sangi, R., Sreenivas, B. S., & Shanker, K. (2023). Mix design of fly ash and GGBS based geopolymer concrete activated with water glass. Engineering, Technology & Applied Science Research, 13(5), 11884–11889. https://doi.org/10.48084/etasr.6216.

Saranya, P., Nagarajan, P., & Shashikala, A. P. (2021). Seismic performance of geopolymer concrete beam-column joints under reverse cyclic loading. Innovative Infrastructure Solutions, 6(2), 92. https://doi.org/10.1007/s41062-021-00474-4.

Sbahieh, S., McKay, G., Nurdiawati, A., & Al-Ghamdi, S. G. (2025). The sustainability of partial and total replacement of Ordinary Portland Cement: A deep dive into different concrete mixtures through life cycle assessment. Journal of Building Engineering, 108, 112830. https://doi.org/10.1016/j.jobe.2025.112830.

Shakir, N., & Dawood, A. (2024). Flexural Behavior of Geopolymer RC Concrete Beams Containing Pet Waste as Sand Replacement. Civil and Environmental Engineering, 21(1), 182–205. https://doi.org/10.2478/cee-2025-0015.

Shen, X., Li, B., & Chen, Y.-T. (2024). Seismic performance of reinforced concrete beam-column joints with diagonal bars wrapped by steel tubes: experimental, numerical and analytical study. Structures, 59, 105734. https://doi.org/10.1016/j.istruc.2023.105734.

Su, X., Yang, H., Liu, Q., Wang, X., & Fu, J. (2024). Experimental study on seismic behavior of reinforced concrete exterior beam-column joints under varying axial load. Engineering Structures, 318, 118682. https://doi.org/10.1016/j.engstruct.2024.118682.

Sumajouw, D. M. J., Hardjito, D., Wallah, S. E., & Rangan, B. V. (2007). Fly ash-based geopolymer concrete: study of slender reinforced columns. Journal of Materials Science, 42(9), 3124–3130. https://doi.org/10.1007/s10853-006-0523-8.

Taheri, A., Moghadam, A. S., & Tasnimi, A. A. (2017). Critical factors in displacement ductility assessment of high-strength concrete columns. International Journal of Advanced Structural Engineering, 9(4), 325–340. https://doi.org/10.1007/s40091-017-0169-6.

Ugale, A. B., & Khante, S. N. (2020). Study of energy dissipation of reinforced concrete beam-column joint confined using varying types of lateral reinforcements. Materials Today: Proceedings, 27, 1356–1361. https://doi.org/10.1016/j.matpr.2020.02.690.

Vamvatsikos, D., & Aschheim, M. A. (2016). Performance- based seismic design via yield frequency spectra. Earthquake Engineering & Structural Dynamics, 45(11), 1759–1778. https://doi.org/10.1002/eqe.2727.

Velastegui, L., Velasco, N., Sanchez Quispe, H. R., Barahona, F., Onyelowe, K. C., Hanandeh, S., Ebid, A. M., & John, T. A. (2024). Predicting the impact of adding metakaolin on the flexural strength of concrete using ML classification techniques–a comparative study. Frontiers in Built Environment, 10, 1434159. https://doi.org/10.3389/fbuil.2024.1434159.

Vijai, K., Kumutha, R., & Vishnuram, B. G. (2010). Effect of types of curing on strength of geopolymer concrete. International Journal of the Physical Sciences, 5(9), 1419–1423.

Wang, Z., Huang, J., Chang, Z., & Lu, Y. (2022). Experimental and Numerical Investigation on Seismic Performance of RC Exterior Beam- Column Joints with Slabs. Shock and Vibration, 2022(1), 3679431. https://doi.org/10.1155/2022/3679431.

Yang, X., Dong, Y., Liu, X., Qiu, T., & Zhou, J. (2024). Seismic Behavior of Concrete Beam-Column Joints Reinforced with Steel-Jacketed Grouting. Buildings (2075-5309), 14(10). https://doi.org/10.3390/buildings14103239.

Zhang, Haiyan, Wan, Keyue, Wu, Bo, & Hu, Zhonghao. (2021). Flexural behavior of reinforced geopolymer concrete beams with recycled coarse aggregates. Advances in Structural Engineering, 24(14), 3281–3298. https://doi.org/10.1177/13694332211026224.

Zhang, X., & Li, B. (2021). Seismic performance of exterior reinforced concrete beam-column joint with corroded reinforcement. Engineering Structures, 228, 111556. https://doi.org/10.1016/j.engstruct.2020.111556.